THE JOURNAL OF PHYSICAL CHEMISTRY C

Article

pubs.acs.org/JPCC

ZnO Micro/Nanocrystals with Tunable Exposed (0001) Facets for Enhanced Catalytic Activity on the Thermal Decomposition of Ammonium Perchlorate

Gen Tang,[†,⊥] Shouqin Tian,[§,‡] Zhaoxia Zhou,[‡] Yanwei Wen,[†] Aimin Pang,[⊥] Yungang Zhang,[⊥] Dawen Zeng,*[,†,‡] Haitao Li,[‡] Bin Shan,*[,†] and Changsheng Xie[‡]

[†]State Key Laboratory of Materials Processing and Die & Mould Technology, and [‡]Nanomaterials and Smart Sensors Research Lab (NSSRL), Department of Materials Science and Engineering, Huazhong University of Science and Technology (HUST), No. 1037, Luoyu Road, Wuhan 430074, People's Republic of China

[§]State Key Laboratory of Silicate Materials for Architectures, Wuhan University of Technology, No. 122, Luo-shi Road, Wuhan, 430070, People's Republic of China

[⊥]HuBei Institute of Aerospace Chemotechnology, No. 58, Qinghe Road, Xiangyang 441003, People's Republic of China

Supporting Information

ABSTRACT: ZnO micro/nanocrystals with different percentages of the exposed (0001) facets were synthesized by a facile chemical bath deposition method. Various characterizations were carried out to understand the relationship between particle shape, exposed (0001) facets, and catalytic activity of ZnO nanocrystals for the thermal decomposition of ammonium perchlorate (AP). An enhancement in the catalytic activity was observed for the ZnO micro/nanocrystals with a higher percentage of the exposed (0001) facets, in which the activation energy E_a of AP decomposition was lowered from 154.0 ± 13.9 kJ/mol to 90.8 ± 11.4 kJ/mol, 83.7 ± 15.1 kJ/mol, and 63.3 ± 3.7 kJ/mol for ZnO micro/nanocrystals with ca. 18.6%, 20.3%, and 39.3% of the exposed (0001) facets. Theoretically evidenced by density functional theory calculations, such highly exposed (0001) facets can be favorable for the adsorption and diffusion of perchloric acid, and also facilitate the formation of active oxygen which can lead to the oxidation reaction of ammonia more completely in the catalytic decomposition of AP.

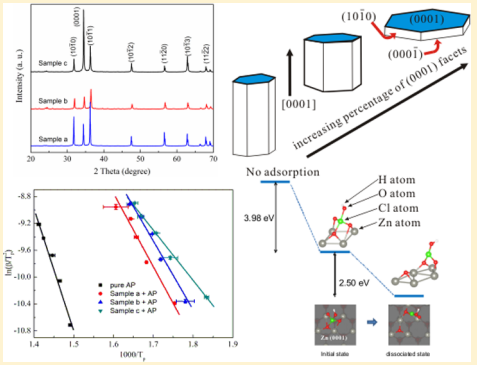

1. INTRODUCTION

Ammonium perchlorate (AP) is the most widely used oxidant in composite solid rocket propellant, generally accounting for 60%−90% of the total mass of the propellant.[1] The thermal decomposition process of AP puts a great impact on the combustion process of the propellant. Several significant parameters for the thermal decomposition of AP, such as activation energy, the rate, and temperature of high-temperature decomposition (HTD), have a close relationship with the combustion performance of solid propellant, especially the burning rate. The lower the HTD temperature is, the shorter is the propellant ignition delay time, and the higher is the burning rate.[2] Therefore, a variety of catalysts have been investigated to anticipate their catalytic properties for the thermal decomposition process of AP.[1−3] Especially, the use of transition metal oxides as a catalyst to increase burning rate has become an effective way.[3−6]

Among these transition metal oxides, zinc oxide (ZnO) has attracted much attention because of its low cost, abundant synthesis, various morphologies, and environment-friendliness.[7] Recently, various nanostructures of ZnO have been applied in the catalytic decomposition of AP and showed excellent catalytic activities.[8−10] For example, hierarchically complex hollow cage-like superstructures assembled by ZnO nanorods have been prepared by Yin[8] and decreased the decomposition temperature of AP to as low as 285 °C, which is lower than the decomposition temperature of AP catalyzed by nanoparticles reported in recent literature reports.[4,10] However, the catalytic mechanism is not quite clear but indeed depends on the surface of ZnO,[10] on which the products of AP decomposition will be adsorbed. The surface of ZnO depends deeply on its crystal structure which can be theoretically constructed as a hexagonal rod with six equivalent nonpolar {10−10} facets exposed on the side surfaces and (0001)/(000−1) facets on the top/bottom facets.[11−13] Both theoretical and experimental investigations have exhibited that the (0001) plane of ZnO is much more reactive than these thermodynamically stable {10−10} facets, which may be the dominant active sites for various applications.[13−17] Unfortunately, most of the prepared ZnO nanocrystals are mainly enclosed by the less-reactive {10−10} facets, which have attracted much interest in the synthesis of ZnO with exposed (0001) facets. Recently, ZnO nanosheets

Received: April 10, 2014
Revised: May 11, 2014
Published: May 12, 2014

with exposed (0001) facets have been prepared, and the correlation between exposed facets and photocatalytic/gas-sensing properties has also been investigated.[16−20] However, there are very few reports focusing on the catalytic activity of ZnO with exposed (0001) facets for the thermal decomposition of AP. In addition, ZnO with different morphologies exhibits a great difference in their catalytic activities for AP decomposition.[8−10,21] Therefore, a good understanding of the correction between the exposed facets of ZnO and catalytic activity for AP decomposition is essential to further enhance the catalytic performance.

In this study, ZnO micro/nanocrystals with different percentages of the exposed (0001) facets were prepared by a facile chemical bath deposition method and applied in promoting the thermal decomposition of AP. An enhancement in the catalytic activity for AP decomposition was observed for ZnO micro/nanocrystals with a higher percentage of the exposed (0001) facets, lowering the activation energy of AP decomposition from 154.0 ± 13.9 kJ/mol to 90.8 ± 11.4 kJ/mol, 83.7 ± 15.1 kJ/mol, and 63.3 ± 3.7 kJ/mol for the ZnO crystals with ca. 18.6%, 20.3%, and 39.3% percentage of exposed (0001) facets. Moreover, in the presence of ZnO nanocrystals with 39.3% percentage of exposed (0001) facets, the HTD temperature of AP was reduced by 125 °C and the heat release was increased by 449 $J \cdot g^{-1}$. It is also confirmed by first-principles calculations that such highly exposed (0001) facets can be favorable for the diffusion of perchloric acid, and also facilitate the formation of active oxygen which can lead to the oxidation reaction of ammonia more completely in the catalytic decomposition of AP.

2. EXPERIMENTAL SECTION

2.1. Sample Preparation. Zinc acetatedehydrate ($Zn(CH_3COO)_2 \cdot 2H_2O$) and absolute methanol (CH_3OH) were analytical grade and used without further purfication. All samples were synthesized according to the following experimental procedure in our previous reports.[12] A 0.6586 g portion (0.003 mol) of zinc acetatedehydrate was dissolved in 30 mL of methanol solution under vigorous stirring at room temperature. The mixture was ultrasonicated for 10 min to obtain a transparent solution. A certain amount of distilled water was added into the above mixed solution. The volume ratios of water/alcohol were 1:6, 1:4, and 1:2, respectively. The beakers were put into a water tank with a constant temperature of 60 °C for 24 h, and then taken out and cooled to the room temperature.[12] Some white precipitate was deposited on the bottom of beakers. Next the white precipitate was cleaned several times by ethanol and distilled water. Then the obtained white powder was calcined in a muffle furnace at 150 °C for 2 h. The ZnO samples with the water/alcohol ratio of 1:6, 1:4, and 1:2 were denoted as Sample a, Sample b, and Sample c, respectively.

2.2. Sample Characterization. Powder X-ray diffraction (XRD) patterns were collected from the prepared samples on a Philips X'Pert Pro X-ray diffractometer (PANalytical, Holland) employing Cu Kα1 radiation (λ = 0.15418 nm). The detailed testing conditions were described as follows. The scan rate (2θ) was 0.05° s^{-1}, the accelerating voltage was 40 kV, the applied current was 80 mA. Field-emission scanning electron microscopy (FESEM) measurements were performed on a FEI Sirion 200 microscope (FEI company, The Netherlands) with an acceleration voltage of 20.0 kV.

The as-prepared samples were studied as a catalyst in the thermal decomposition of AP (AR, d50:135 μm). The catalytic roles of ZnO in the thermal decomposition of AP were studied by TG-DTA test using Diamond TG/DTA in N_2 atmosphere over the temperature range of 30−500 °C.[21]

To investigate the catalytic roles of ZnO samples on AP decomposition, Sample a, Sample b, Sample c, and AP were premixed in a mass ratio of 4:100 respectively for the TG-DTA test at a heating rate of 10 K/min. The activation energies of AP decomposition with and without additives of ZnO were measured by varying the heating rates to further compare the catalytic properties of ZnO samples with different morphologies on the AP decomposition.[4] To investigate the influence of the dosage of ZnO samples on the AP decomposition, AP and ZnO were premixed at a mass ratio ranging from 100:1 to 100:5 to prepare the target samples. A total sample mass of 3.0 mg was used for all runs.

3. RESULTS AND DISCUSSION

3.1. Structure of as-Prepared Samples. Figure 1 shows XRD patterns of Sample a, Sample b, and Sample c. It can be seen that all diffraction peaks are in good agreement with the hexagonal ZnO structure with the lattice constants a = 0.3249 nm and c = 0.5206 nm, compatible with the literature values of JCPDS No. 36-1451. The diffraction peaks are very sharp, implying high crystalline of samples. In the JCPDS 36-1451 card, the relative diffraction intensities of the (10−10) plane and (10−11) plane are higher than that of the (0001) facet. However, the diffraction intensity ratio of the (0001) polar plane to the (10−10) nonpolar plane ($I_{(0001)}/I_{(10-10)}$) is 0.729, 1.160, and 4.860 for Sample a, Sample b, and Sample c, respectively, indicating increased (0001) facets in the particles with an increase in the volume ratio of H_2O/methanol.[17]

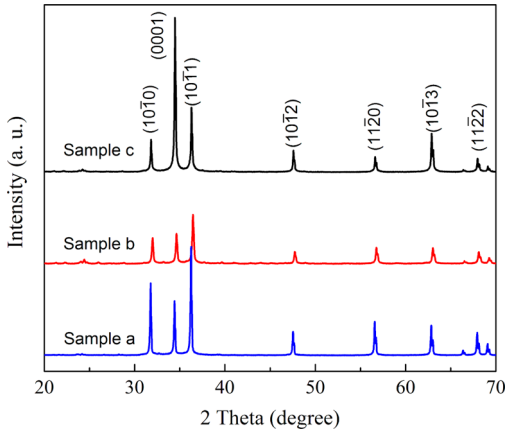

Figure 1. XRD patterns of Sample a, Sample b, and Sample c.

The FESEM images of the as-prepared samples are shown in Figure 2. It can be seen that the morphology evolution of ZnO depends deeply on the volume ratio of H_2O/methanol. When the volume ratio is 1:6, Sample a shows hexagonal columnar morphology with an average size of ca. 410 nm and a thickness of 310 nm (Figure 2a). On the basis of the above structure information including the XRD results, the geometry of Sample a can be considered as hexagonal columnar with (0001)/(000−1) facets at the top/bottom and (10−10) facets on the side as shown in Figure 2d. The calculated percentage of exposed (0001) facets is ca. 18.6%. With the volume ratio of 1:4, Sample

dx.doi.org/10.1021/jp503510x | J. Phys. Chem. C 2014, 118, 11833−11841

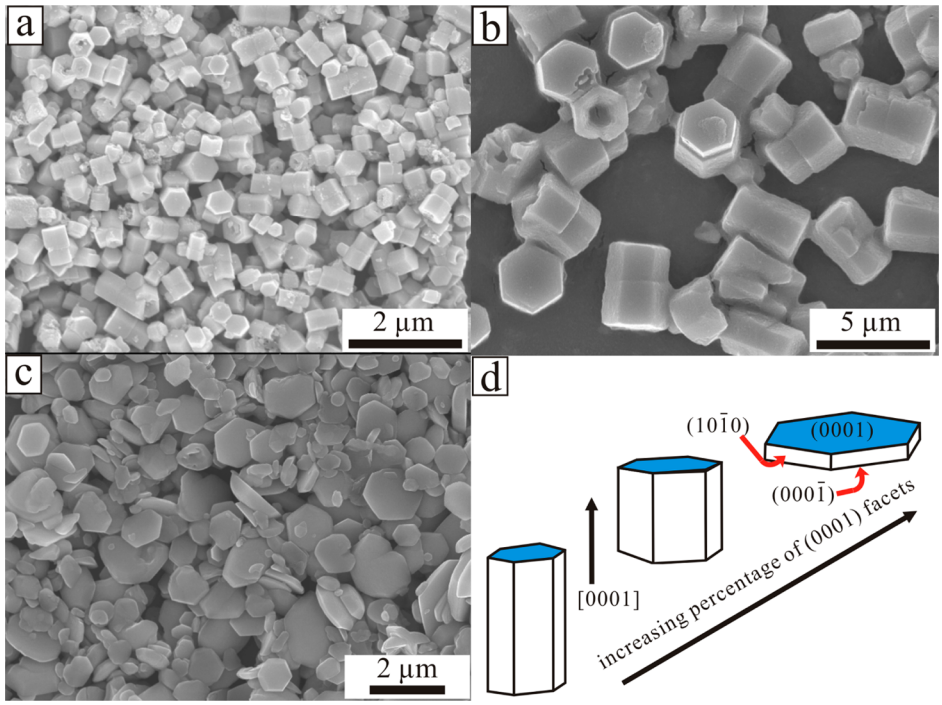

Figure 2. FE-SEM images of (a) Sample a, (b) Sample b, and (c) Sample c; (d) the changes in the percentage of (0001) facets at the surface of different shapes.

b has no obvious changes in their shapes while their size and thickness are increased to ca. 2.74 μm and ca. 1.73 μm, respectively (Figure 2b). The percentage of exposed (0001) facets is estimated to be ca. 20.3%. Furthermore, as the volume ratio increases to 1:2, Sample c exhibits a hexagonal plate with an average diameter of ca. 1.10 μm and a thickness of ca. 130 nm (Figure 2c), and a higher percentage of exposed (0001) facets (ca. 39.3%). It is noted that the top surface of the nanoplates is not flat and there are probably {01−11} facets included according to our previous report.[12] However, the proportion of the {01−11} facets is very small and is difficult to determine compared with that of (0001), (000−1), and {10−10} facets. Moreover, {01−11} facets cannot be observed in Sample a and Sample b. Thus, the proportion of the {01−11} facets cannot be calculated in Table 1. But the role of {01−11} facets in the catalytic activity for AP decomposition will be also considered and discussed later. It can be concluded that in our experiment the size and shape of ZnO particles can be controlled well by adding H_2O, which not only controls the hydrolysis of $Zn(CH_3COO)_2$, but also affects the nucleation process of ZnO significantly. The detailed growth mechanism is described in our previous work.[12] With an increase of H_2O/methanol volume ratio, the ratio of thickness/diameter is decreased, and ZnO also shows an obvious morphology change from rod to plate and a higher percentage of exposed (0001) facets, as shown in Table 1.

Table 1. Calculated Percentage of Exposed (0001) Facets for the as-Prepared Samples

	average diameter (μm)	average thickness (μm)	calculated area of (0001) facet (m^2/g)	calculated area of total surface (m^2/g)	percentage of exposed (0001) facet (%)
Sample a	0.41	0.30	0.59	3.20	18.6
Sample b	2.74	1.73	0.10	0.51	20.3
Sample c	1.10	0.13	1.37	3.49	39.3

Detailed Method. Tens of ZnO particles in Figure 2 have been chosen to calculate the average diameter and thickness. These samples exhibit a hexagonal columnar shape, and thus the maximum length on the hexagonal surface is considered as the diameter, the distance between the top hexagonal surface and the bottom surface is defined as the thickness of a ZnO particle. According to the calculated average diameter (D) and thickness (h), the hexagonal surface is a (0001) or (000−1) facet, and its area is equivalent to $3^{3/2}D^2/8$, the side surface is a {10−10} facet, and its area can be calculated as $3Dh$. The volume of the nanorod or nanoplate can be calculated as $3^{3/2}hD^2/8$. In this sense, the specific surface area and area of (0001) facets can be calculated as $(3^{3/2}D^2/4 + 3Dh)/(\rho 3^{3/2}hD^2/8)$ and $1/\rho h$, respectively. The percentage of the (0001) facet can be calculated as $3^{3/2}D^2/[8*(3^{3/2}D^2/4 + 3Dh)]$. Here, ρ is the density of ZnO and can get the value of 5.606 g/cm^3.

To further determine the polar direction of samples, ZnO nanoplates were selected and subjected to the convergent beam electron diffraction (CBED) characterization. As is well-known, the polarity of ZnO nanoplates can be determined by CBED according to the asymmetry in the diffraction pattern.[22,23] A low-magnified TEM image of ZnO nanoplates is shown in Figure 3a. The CBED pattern acquired at the body (marked with b) of the nanoplates is given in Figure 3b. The asymmetry of the (0002) and (000−2) spots can be seen, confirming the polarity of ZnO nanoplates. The simulated CBED pattern is calculated under the assumption that the exposed top facet of the nanoplate is the (0002) plane in Figure 3c, and the pattern is consistent with the experimental results. This shows that the top surface of the ZnO nanoplates corresponds to the (0002) facet. According to the polarity of the ZnO nanoplate, the exposed bottom surface is the (000−2) facet. It can be seen

dx.doi.org/10.1021/jp503510x | J. Phys. Chem. C 2014, 118, 11833−11841

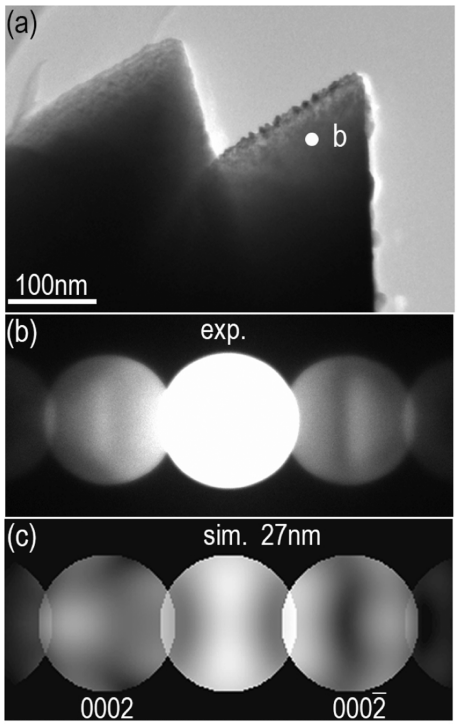

Figure 3. (a) TEM image and (b) the convergent beam electron diffraction (CBED) patterns obtained on the ZnO nanoplates along the [01−10] zone axis; (c) the corresponding simulated CBED pattern for a crystal thickness of 27 nm.

that the two exposed facets exhibit a similar surface area. In this sense, the surface area of (0001) facet is a half of the total surface area of end surfaces including (0001) facets and (000−1) facets, and can be calculated in Table 1.

3.2. Catalytic Activity of ZnO for Thermal Decomposition of AP. The as-prepared ZnO samples with different percentages of exposed (0001) facets were initially studied as an additive to promote the thermal decomposition of AP with an attempt to understand their catalytic properties. The performance of ZnO in the thermal decomposition of AP was investigated by TG-DTA measurements.

Figure 4 shows the DTA curves of both pure AP and the mixture of AP with different ZnO samples at a 4% mass basis and a heating rate of 10 K/min. Only two thermal signals are

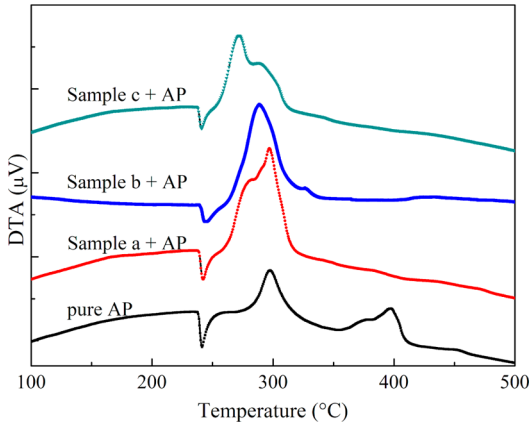

Figure 4. DTA curves of pure AP and AP with ZnO samples at a heating rate of 10 K/min.

observed for the mixture of AP with ZnO samples compared to three obvious peaks for pure AP. The first endothermic peak of all the four curves at 240−245 °C is due to the crystal transformation of AP from orthorhombic to cubic phase.[10] It can be seen clearly from the DTG curves (Figure 5) of pure AP

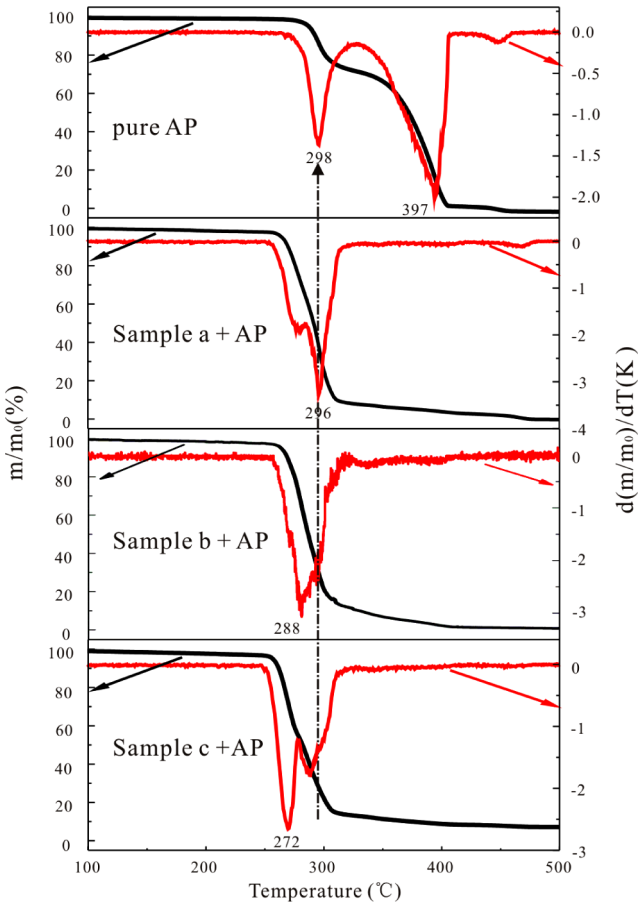

Figure 5. TG and DTG curves of pure AP and AP with ZnO samples at 10 K/min.

that there are two obvious exothermic peaks centered at about 298 and 397 °C, which correspond to the low-temperature decomposition (LTD) and HTD, respectively. The LTD has been proposed to be a heterogeneous process which includes a proton transfer in the AP subsurface to yield NH_3 and $HClO_4$, the adsorption of NH_3 and $HClO_4$ in the porous structure, and finally the decomposition of $HClO_4$ and oxidation of NH_3. Alternatively, the HTD process is due to the oxidation of NH_3 by $HClO_4$ in the closed sample pans.[1,2,10]

After involving the as-prepared ZnO samples, a significant difference for AP decomposition is the obvious reduction of the HTD temperature. In the presence of Sample a, Sample b, and Sample c, the HTD temperature is reduced by 101 °C, 109 °C, and 125 °C (Figure 5), and the heat release increases from 574 J/g to 1109, 971, and 1033 J/g (Figure 4), respectively. These results suggest that the ZnO catalyst can greatly promote the thermal decomposition of AP, and Sample c with a higher percentage of exposed (0001) facets shows a better catalytic activity for thermal decomposition of AP than Sample a and Sample b. This is probably related to the percentage of exposed (0001) facets, which will be discussed later.

To further study catalytic properties of the different ZnO samples for the thermal decomposition of AP, Sample a,

dx.doi.org/10.1021/jp503510x | J. Phys. Chem. C 2014, 118, 11833−11841

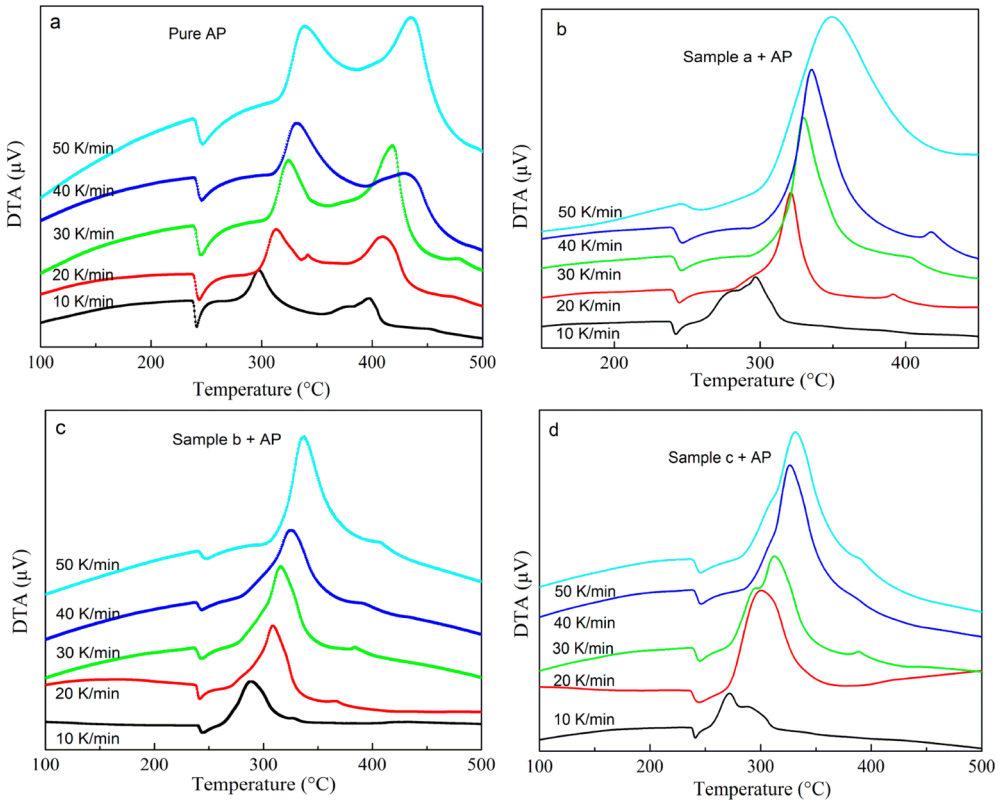

Figure 6. DTA curves of (a) pure AP and (b–d) AP with 4 wt % as-prepared ZnO samples at different heating rates.

Sample b, and Sample c were premixed with AP in a mass ratio of 4:100, respectively, for DTA test at different heating rates. Figure 6 shows the DTA curves of the mixtures of AP with the samples at different heating rates in crucibles with lids. It is found that the decomposition temperature of AP without (Figure 6a) or with ZnO additives (Figure 6b–d) is dependent on the heating rate. With an increase of heating rate, the crystal transition temperature of AP thermal decomposition has no obvious change, but the temperature of the LTD and HTD processes increases obviously. From the exothermic peak temperature as a function of heating rate, several important kinetic parameters for AP decomposition with ZnO additives can be calculated.[21] The relationship between decomposition temperature of AP and heating rate can be described by the Kissinger correlation:[4,21]

$$\ln\left(\frac{\beta}{T_p^2}\right) = \ln\left(\frac{AR}{E_a}\right) - \frac{E_a}{RT_p} \quad (1)$$

where β is the heating rate in degrees Celsius per minute, T_p is the peak temperature, R is the ideal gas constant, E_a is the activation energy, and A is the pre-exponential factor. According to eq 1, the term $\ln(\beta/T_p^2)$ varies linearly with $1/T_p$, yielding the kinetic parameters of activation energy from the slope of the straight line and of pre-exponential factor from the intercept. Figure 7 shows the experimentally measured $\ln(\beta/T_p^2)$ versus $1/T_p$ with and without ZnO additives. For pure AP, the activation energy of HTD was calculated to be 154.0 ± 13.9 kJ/mol, which is close to the value previously reported in the literature.[4,21] In the presence of ZnO additives, the activation energy of AP decomposition becomes as small as E_a = 90.8 ± 11.4 kJ/mol with Sample a, 83.7 ± 15.1 kJ/mol with Sample b, or 63.3 ± 3.7 kJ/mol with Sample c. Obviously, the ZnO

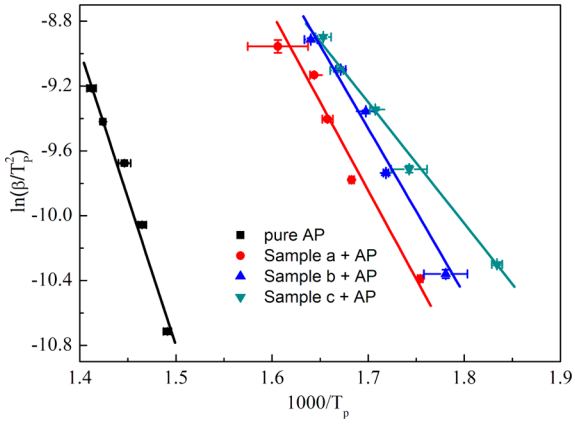

Figure 7. Dependence of $\ln(\beta/T_p)$ on $1/T_p$ for AP and mixtures of AP with 4 wt % ZnO additives. Scatter points are experimental data and lines denotes the linear fitting results.

samples with different percentages of exposed (0001) facets can entirely promote the thermal decomposition of AP, and the catalytic effect of ZnO samples lies in the order of Sample a < Sample b < Sample c. This shows that the morphologies of ZnO, especially the exposed (0001) facets, play an important role in the catalytic properties for the thermal decomposition of AP.

3.3. The Relationship between Polar Planes and Catalytic Activity of ZnO. According to the catalytic mechanism for the thermal decomposition of pure AP proposed by Jacobs,[24] the first decomposition step is a solid–gas multiphase reaction including low-temperature decomposition and high-temperature decomposition as follows:[10]

dx.doi.org/10.1021/jp503510x | J. Phys. Chem. C 2014, 118, 11833–11841

$$NH_4^+ClO_4^- \Leftrightarrow NH_3—H—ClO_4$$
$$\Leftrightarrow NH_3—HClO_4$$
$$\Leftrightarrow NH_{3(a)} + HClO_{4(a)}(LTD) \quad (2)$$

$$NH_{3(a)} + HClO_{4(a)} \Leftrightarrow NH_{3(g)} + HClO_{4(g)}(HTD) \quad (3)$$

$NH_4^+ClO_4^-$ corresponds to the pair of ions (NH_4^+ and ClO_4^-) in the AP lattice. The low-temperature decomposition has been proposed to be a heterogeneous process which includes a proton transfer from the cation NH_4^+ to the anion ClO_4^- in the AP subsurface to yield NH_3 and $HClO_4$, the adsorption of NH_3 and $HClO_4$ in the porous structure, and finally the decomposition of $HClO_4$ and reaction with NH_3.[10] Alternatively, the high-temperature exothermic process is due to the oxidation of NH_3 by $HClO_4$ in the gas phase.[1,2,10]

For pure AP, at the LTD process, the reaction of the surface proceeds more rapidly than sublimation. And the rate of ammonia outflow from pores of AP is about 2.5 times higher than that of perchloric acid (PA).[1,25,26] As the ratio of NH_3 to $HClO_4$ decreases continuously in pores, the accumulation of perchloric acid will cause the shift of the proton equilibrium to the left-hand side, which can account for the cessation of such a reaction.[4,10] For the reaction proceeding in the adsorbed layer, it is assumed that perchloric acid is desorbed more rapidly than ammonia. In addition, oxidation of ammonia becomes incomplete and thus the surface gets saturated with ammonia, also accounting for cessation of the reaction and incomplete transformation of perchlorate.[1]

As discussed above, PA is the key chain carriers in the decomposition of AP in its incipient stages, since PA is adsorbed in the pores of AP and prevents the continuous decomposition of AP.[27−29] Catalysts such as ZnO have been introduced to promote the reaction of PA to boost the decomposition of AP. PA will be adsorbed on the surface of ZnO at first and then dissociate. In this sense, the exposed facets of ZnO nanocrystals will play an important role in the adsorption and decomposition of PA. The most common planes of hexagonal ZnO are the Zn-(0001), O-(000−1) polar planes and the (10−10) nonpolar surface.[27,28] The oppositely charged ions produce positively charged Zn^{2+} (0001) and negatively charged O^{2-} (000−1) polar surfaces.[11,28] Under thermodynamic equilibrium conditions, the higher-surface-energy facet is usually small in area, while the lower-energy facets are larger.[12] The Zn (0001) plane, which holds the highest surface energy, is inherently more reactive than O (000−1) or nonpolar {01−10}.[11,12] Owing to the charge interaction and lower surface energy, O (000−1) and nonpolar {01−10} planes are probably poorer in adsorbing $HClO_4$ and NH_3 gases than the Zn (0001) plane, resulting in a lower activity.[28] However, the fundamental question of how this happens has not been answered. To clarify this, density functional theory (DFT) calculations and the nudged elastic band method (NEB) are used to study the adsorption and decomposition of PA on the surfaces of ZnO, that is, the {10−10} and (0001) facets. The models of ZnO for (0001) and (10−10) facets are shown in Figure 8 panels a and b, respectively. DFT calculations were carried out using plane waves as implemented in the Vienna Ab-initio Simulation Package.[29−31] The cutoff energy of the electronic wave functions were expanded to 400 eV, and projected augmented wave function (PAW) pseudopotentials[32] were used to describe electron−ion interactions. The Perdew−Burke−Ernzerhof

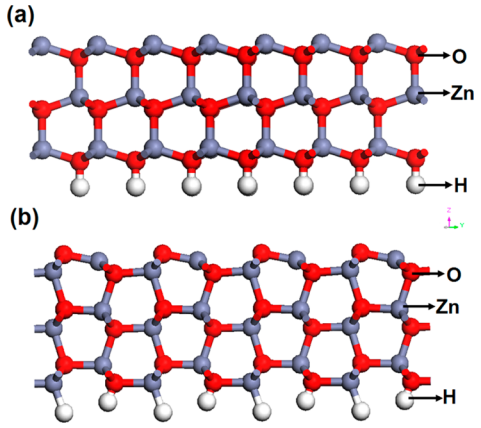

Figure 8. Surface models of (0001) and (10−10) facets of ZnO.

(PBE) functional[33] was used as an exchange-correlation functional. The geometry optimization is considered complete when the Hellmann−Feynman force on each atom is less than 0.05 eV/Å. A climbing nudged elastic band (NEB) calculation[34,35] is used to calculate the minimum energy path (MEP) and find the saddle points between two local minima for the system. For the relaxed ZnO (10−10) slab (Figure 8b), oxygen atoms on the surface stick slightly out of plane. Three possible adsorption configurations were considered for $HClO_4$ adsorption, as shown in Figure 9a. The adsorption energies for

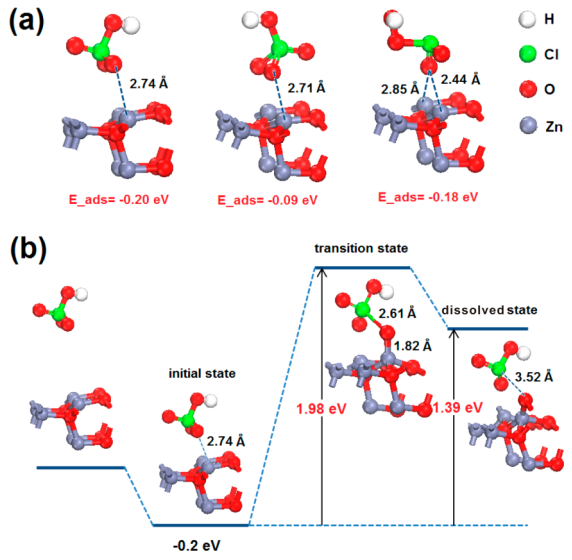

Figure 9. (a) The adsorption geometries and (b) dissociation path of $HClO_4$ on ZnO (10−10) facets.

these three geometries are −0.20, −0.09, and −0.18 eV, respectively, which indicate the adsorption of PA on the ZnO (10−10) is relatively weak. The most stable ground state corresponds to a configuration where two oxygen atoms in the percolate make bonds with two Zn atoms on the surface. Figure 9b shows the MEP for such a process starting from the most stable adsorption geometry. The transition state corresponds to a midpoint along the pathway where the O−Cl bond is partially broken while the oxygen atom is migrating over the top site to the more stable 2-fold coordinated bridge site. The activation barrier deduced from the energy difference between transition state and initial state is 1.98 eV, which is relatively high. This

dx.doi.org/10.1021/jp503510x | J. Phys. Chem. C 2014, 118, 11833−11841

indicates that such a decomposition process seems to be impractical on an ideal ZnO (10−10) surface. For a ZnO (0001) slab (Figure 8a), there are four possible adsorption configurations for $HClO_4$ adsorption, as shown in Figure 10a.

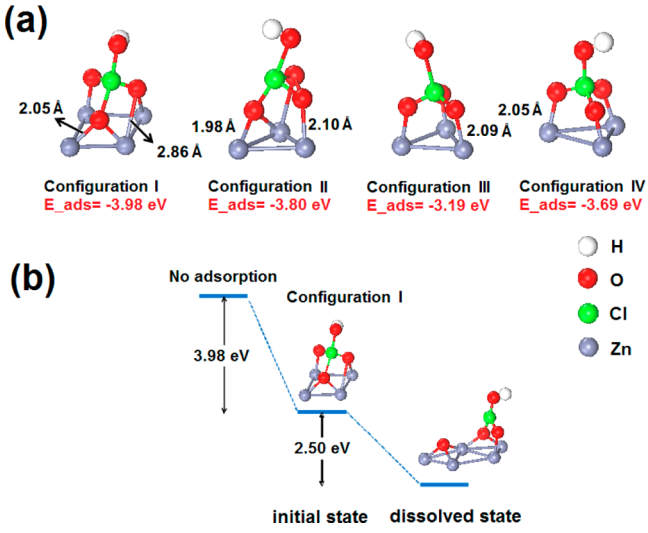

Figure 10. (a) The adsorption geometries and (b) dissociation path of $HClO_4$ on ZnO (0001) facets.

The adsorption energies for these four geometries are −3.98, −3.80, −3.19 eV, and −3.69 eV, respectively, which indicate the adsorption of PA on the ZnO (0001) facets is easier than that of the (10−10) facets. The adsorption configuration I is the most stable, and this adsorption is also a spontaneous process. Also, it can be seen from Figure 10b that PA starts to decompose when its O−Cl bond is partially broken and the active oxygen atom is thus formed. The formation energy of oxygen atoms is −2.50 eV, indicating that this process can be carried out automatically. On the basis of these calculation results, it is easier for PA adsorption and the formation of an active oxygen atom on the (0001) facets than on the (10−10) facets under the same conditions. It is noted that Sample c has a few {01−11} facets while Sample a and Sample b do not. The role of the {01−11} facets in the catalytic decomposition of AP is also revealed through DFT calculations as shown in Supporting Information, Figure S1. The adsorption of $HClO_4$ (the important initial intermediate product of AP) on the (01−11) surface behaves similarly with that of the (0001) facet. However, the binding energy is calculated to be −3.51 eV, which is weaker than that of the (0001) surface (−3.98 eV). In this sense, {01−11} facets can promote the thermal decomposition of AP better than {10−10} facets but weaker than the (0001) facet. Therefore, Sample c with a larger pencentage of (0001) facet and a few {01−11} facets exhibits better catalytic activity for AP decomposition than Sample a and Sample b.

In the other hand, the conduction-band electrons (e_{cb}^-) can be generated on the surfaces of ZnO at a temperature of about 250 °C when ZnO is excited by a heating energy greater than the band gap energy.[36,37] If the surface charges are uncompensated, the net dipole moment tends to diverge and the electrostatic potential increases. The polarity of gaseous $HClO_4$ is stronger than that of gaseous NH_3. Owing to charge interactions, the negatively charged $HClO_4$ (g) were preferentially adsorbed on the positively charged Zn^{2+} (0001) surfaces of ZnO.[28] The positive holes and corresponding active sites in ZnO are highly associated with the adsorption of electron exchange.[11] The perchloric acid acts as an electron acceptor by forming a superoxide radical anion O^- (eq 4). As a result, the reverse reaction was held back during decomposition of the perchlorates.

$$e_{cb}^- + HClO_4 \rightarrow HClO_x\ (x = 0, 1, 2, 3) + O^- \quad (4)$$

The oxygen negative ion (O^-) species are more stable above 200 °C than O^{2-}, and have higher oxidizability and activity as an O source than O_2. The oxygen negative ion (O^-) with powerful oxidation ability can react with NH_3 (eq 5). Simultaneously, a series of reactions which increases the exothermic heat of the thermal decomposition process occur on the surface of ZnO.

$$NH_3 + O^- \rightarrow N_2O + H_2O \quad (5)$$

In summary, ZnO samples should be considered as the catalyst accelerating both the diffusion of perchloric acid and the formation of O^- which leads to the oxidation reaction of ammonia more completely. It is therefore concluded that the exposed (0001) polar plane of ZnO is the most active site for the catalytic decomposition of AP.

As can be seen from the data in Table 1, the samples with respect to the proportion of exposed (0001) polar surface in the total surface area lie in the order of Sample a < Sample b < Sample c, which is consistent with the order of their catalytic effect for AP decomposition. This order occurs because, the greater is the proportion of exposed (0001) polar facets, that is, the greater is the proportion of Zn surfaces, the more $HClO_4(g)$ would be preferentially adsorbed on the Zn surfaces. This will accelerate reaction 3 and expedite the diffusion of $HClO_4$. Then the $HClO_4(g)$ will not accumulate in perchlorate to hinder the decomposition reaction. Therefore the decomposition temperature will be reduced, or even the decomposition stage will be concentrated in one step. Meanwhile, the acceleration of reaction 4 can produce more O^- to promote the oxidation of NH_3 and increase the heat release, resulting in the proton equilibrium to the right-hand side.

4. CONCLUSION

ZnO samples with different percentages of the exposed (0001) facets were controllably prepared by a facile chemical deposition method. By adjusting the H_2O/methanol volume ratio, the shape of ZnO particles can be readily tailored from hexagonal prism into hexagonal plate and the proportion of exposed (0001) polar planes of ZnO nanocrystals increases. The as-prepared samples were explored as the catalysts to promote the AP decomposition. It was found that the HTD temperature of AP apparently decreased followed by a significant increase in the decomposition heat. More importantly, the different samples showed a morphology-dependent activity: ZnO nanocrystals with a higher percentage of exposed (0001) facets are more catalytically active for the reaction. This was because that the exposed (0001) facets can not only accelerate the adsorption and diffusion of perchloric acid, but also facilitate the formation of O^- which leads to the oxidation reaction of ammonia more completely, thus promoting the thermal decomposition of AP. This work can provide new insights to enhance the catalytic activity of oxide nanoparticles for AP decomposition.

dx.doi.org/10.1021/jp503510x | J. Phys. Chem. C 2014, 118, 11833−11841

■ ASSOCIATED CONTENT

Supporting Information

The adsorption of the $HClO_4$ molecule (the key chain carriers in the decomposition of AP in its incipient stages) on the ZnO (01−11) surface through DFT calculation. This material is available free of charge via the Internet at http://pubs.acs.org.

■ AUTHOR INFORMATION

Corresponding Author

*Tel.: +86-27-87559835. Fax: +86-27-87543778. E-mail: dwzeng@mail.hust.edu.cn; bshan@mail.hust.edu.cn.

Notes

The authors declare no competing financial interest.

■ ACKNOWLEDGMENTS

This work was supported by the National Basic Research Program of China (Grant Nos. 2009CB939702 and 2009CB939705), and Open Foundation of the State Key Laboratory of Silicate Materials for Architectures at Wuhan University of Technology (No. SYSJJ2013-06). The authors thank Prof. Jianbo Wang and Weiwei Meng at Wuhan Universty for their assistance in the CBED characterization and simulation calculation. Also, the technology was supported by the Analytic Testing Center of HUST for performing XRD and FESEM characterizations.

■ REFERENCES

(1) Boldyrev, V. V. Thermal Decomposition of Ammonium Perchlorate. *Thermochim. Acta* **2006**, *443*, 1−36.

(2) Vyazovkin, S.; Wight, C. A. Kinetics of Thermal Decomposition of Cubic Ammonium Perchlorate. *Chem. Mater.* **1999**, *11*, 3386−3393.

(3) Xu, H.; Wang, X. B.; Zhang, L. Z. Selective Preparation of Nanorods and Micro-octahedrons of Fe_2O_3 and Their Catalytic Performances for Thermal Decomposition of Ammonium Perchlorate. *Powder Technol.* **2008**, *185*, 176−180.

(4) Li, L. P.; Sun, X. F.; Qiu, X. Q.; Xu, J. X.; Li, G. S. Nature of Catalytic Activities of CoO Nanocrystals in Thermal Decomposition of Ammonium Perchlorate. *Inorg. Chem.* **2008**, *47*, 8839−8846.

(5) Wang, Y. P.; Zhu, J. W.; Yang, X. J.; Lu, L. D.; Wang, X. Preparation of NiO Nanoparticles and Their Catalytic Activity in The Thermal Decomposition of Ammonium Perchlorate. *Thermochim. Acta* **2005**, *437*, 106−109.

(6) Reid, D. L.; Russo, A. E.; Carro, R. V.; Stephens, M. A.; LePage, A. R.; Spalding, T. C.; Petersen, E. L.; Seal, S. Nanoscale Additives Tailer Energetic Materials. *Nano Lett.* **2007**, *7*, 2157−2161.

(7) Yang, D. S.; Lao, C.; Zewail, A. H. 4D Electron Diffraction Reveals Correlated Unidirectional Behavior in Zinc Oxide Nanowires. *Science* **2008**, *321*, 1660−1664.

(8) Yin, J. Z.; Lu, Q. Y.; Yu, Z. N.; Wang, J. J.; Pang, H.; Gao, F. Hierarchical ZnO Nanorod-Assembled Hollow Superstructures for Catalytic and Photoluminescence Applications. *Cryst. Growth Des.* **2010**, *10*, 40−43.

(9) Zheng, M.; Wang, Z. S.; Wu, J. Q.; Wang, Q. Synthesis of Nitrogen-Doped ZnO Nanocrystallites with One-Dimensional Structure and Their Catalytic Activity for Ammonium Perchlorate Decomposition. *J. Nanopart. Res.* **2010**, *12*, 2211−2219.

(10) Sun, X. F.; Qiu, X. Q.; Li, L. P.; Li, G. S. ZnO Twin-Cones: Synthesis, Photoluminescence, and Catalytic Decomposition of Ammonium Perchlorate. *Inorg. Chem.* **2008**, *47*, 4146−4152.

(11) Wöll, C. The Chemistry and Physics of Zinc Oxide Surfaces. *Prog. Surf. Sci.* **2007**, *82*, 55−120.

(12) Wang, H. H.; Xie, C. S.; Zeng, D. W. Controlled Growth of ZnO by Adding H_2O. *J. Cryst. Growth* **2005**, *277*, 372−377.

(13) Li, G. R.; Hu, T.; Pan, G. L.; Yan, T. Y.; Gao, X. P.; Zhu, H. Y. Morphology-Function Relationship of ZnO: Polar Planes, Oxygen Vacancies, and Activity. *J. Phys. Chem. C* **2008**, *112*, 11859−11864.

(14) Xu, L. P.; Hu, Y. L.; Pelligra, C.; Chen, C. H.; Jin, L.; Huang, H.; Sithambaram, S.; Aindow, M.; Joesten, R.; Suib, S. L. ZnO with Different Morphologies Synthesized by Solvothermal Methods for Enhanced Photocatalytic Activity. *Chem. Mater.* **2009**, *21*, 2875−2885.

(15) Kurtz, M.; Strunk, J.; Hinrichsen, O.; Muhler, M.; Fink, K.; Meyer, B.; Wöll, C. Active Sites on Oxide Surfaces: ZnO-Catalyzed Synthesis of Methanol from CO and H_2. *Angew. Chem., Int. Ed.* **2005**, *44*, 2790−2794.

(16) Jang, E. S.; Won, J. H.; Hwang, S. J.; Choy, J. H. Fine Tuning of the Face Orientation of ZnO Crystals to Optimize Their Photocatalytic Activity. *Adv. Mater.* **2006**, *18*, 3309−3312.

(17) Tian, S. Q.; Yang, F.; Zeng, D. W.; Xie, C. S. Solution-Processed Gas Sensors Based on ZnO Nanorods Array with an Exposed (0001) Facet for Enhanced Gas-Sensing Properties. *J. Phys. Chem. C* **2012**, *116*, 10586−10591.

(18) Gurlo, A. Nanosensors: Towards Morphological Control of Gas Sensing Activity. SnO_2, In_2O_3, ZnO, and WO_3 Case Studies. *Nanoscale* **2011**, *3*, 154−165.

(19) Mclaren, A.; Valdes-Solis, T.; Li, G. Q.; Tsang, S. C. Shape and Size Effects of ZnO Nanocrystals on Photocatalytic Activity. *J. Am. Chem. Soc.* **2009**, *131*, 12540−12541.

(20) Han, X. G.; He, H. Z.; Kuang, Q.; Zhou, X.; Zhang, X. H.; Xu, T.; Xie, Z. X.; Zheng, L. S. Controlling Morphologies and Tuning the Related Properties of Nano/Microstructured ZnO Crystallites. *J. Phys. Chem. C* **2009**, *113*, 584−589.

(21) Zhou, Z. X.; Tian, S. Q.; Zeng, D. W.; Tang, G.; Xie, C. S. MOX (M = Zn, Co, Fe)/AP Shell−Core Nanocomposites for Self-Catalytical Decomposition of Ammonium Perchlorate. *J. Alloys Compd.* **2012**, *513*, 213−219.

(22) Zhang, J. M.; Zhang, X. Z.; Chen, L.; Xu, J.; You, L. P.; Ye, H. Q.; Yu, D. P. In Situ Study of the Growth of ZnO Nanosheets Using Environmental Scanning Electron Microscope. *Appl. Phys. Lett.* **2007**, *90*, 233104:1−3.

(23) Zhou, X.; Xie, Z. X.; Jiang, Z. Y.; Kuang, Q.; Zhang, S. H.; Xu, T.; Huang, R. B.; Zheng, L. S. Formation of ZnO Hexagonal Micro-Pyramids: A Successful Control of the Exposed Polar Surfaces with the Assistance of an Ionic Liquid. *Chem. Commun.* **2005**, *44*, 5572−5574.

(24) Jacobs, P. W. M.; Russell-Jones, A. Sublimation of Ammonium Perchlorate. *J. Phys. Chem.* **1968**, *72*, 202−207.

(25) Boldyrev, V. V.; Savintzev, Y. P.; Mulina, T. V. On the Mechanism of Formation and Growth of the Nuclei in Thermal Decomposition of Ammonium Salts. Proceedings of the 7th International Symposium on the Reactivity of Solids, Chapmann and Hall: Bristol, UK, 1972; pp 421−430.

(26) Khairetdinov, E. F.; Boldyrev, V. V. The Mechanism of the Low Temperature Decomposition of NH_4ClO_4. *Thermochim. Acta* **1980**, *41*, 63−86.

(27) Shen, G. Z.; Chen, D.; Lee, C. J. Hierarchical Saw-like ZnO Nanobelt/ZnS Nanowire Heterostructures Induced by Polar Surfaces. *J. Phys. Chem. B* **2006**, *110*, 15689−15693.

(28) Zeng, J. H.; Jin, B. B.; Wang, Y. F. Facet Enhanced Photocatalytic Effect with Uniform Single-Crystalline Zinc Oxide Nanodisks. *Chem. Phys. Lett.* **2009**, *472*, 90−95.

(29) Kresse, G.; Hafner, J. Ab initio Molecular Dynamics for Liquid Metals. *Phys. Rev. B* **1993**, *47*, 558−561.

(30) Kresse, G.; Hafner, J. Ab initio Molecular-Dynamics Simulation of the Liquid−Metal−Amorphous-Semiconductor Transition in Germanium. *Phys. Rev. B* **1994**, *49*, 14251−14269.

(31) Kresse, G.; Hafner, J. Efficiency of Ab-Initio Total Energy Calculations for Metals and Semiconductors Using a Plane-Wave Basis Set. *Comput. Mater. Sci.* **1996**, *6*, 15−50.

(32) Kresse, G.; Joubert, D. From Ultrasoft Pseudopotentials to the Projector Augmented-Wave Method. *Phys. Rev. B* **1999**, *59*, 1758−1775.

(33) Perdew, J. P.; Burke, S.; Ernzerhof, M. Generalized Gradient Approximation Made Simple. *Phys. Rev. Lett.* **1996**, *77*, 3865−3868.

(34) Henkelman, G.; Jónsson, H. Improved Tangent Estimate in The Nudged Elastic Band Method for Finding Minimum Energy Paths and Saddle Points. *J. Chem. Phys.* **2000**, *113*, 9978−9985.

(35) Henkelman, G.; Uberuaga, B. P.; Jónsson, H. A Climbing Image Nudged Elastic Band Method for Finding Saddle Points and Minimum Energy Paths. *J. Chem. Phys.* **2000**, *113*, 9901−9904.
(36) Korotcenkov, G. Metal Oxides for Solid-State Gas Sensors: What Determines Our Choice? *Mater. Sci. Eng., B* **2007**, *139*, 1−23.
(37) Mitra, P.; Chatterjee, A. P.; Maiti, H. S. ZnO Thin Film Sensor. *Mater. Lett.* **1998**, *35*, 33−38.